Journal of Power Sources 271 (2014) 285–290

Contents lists available at ScienceDirect

Journal of Power Sources

journal homepage: www.elsevier.com/locate/jpowsour

Improving the performance of high voltage $LiMn_{1.5}Ni_{0.5}O_4$ cathode material by carbon coating

Svetlana Niketic, Martin Couillard, Dean MacNeil, Yaser Abu-Lebdeh*

Energy, Mining and Environment Portfolio, National Research Council of Canada, 1200 Montreal Road, Ottawa ON K1A 0R6, Canada

HIGHLIGHTS

- Synthesis of octadecahedron crystals of high voltage $LiMn_{1.5}Ni_{0.5}O_4$ cathode.
- Carbon coating of crystals from different sources.
- Coating enhances Li-ion battery performance at high cycling rates and temperatures.

GRAPHICAL ABSTRACT

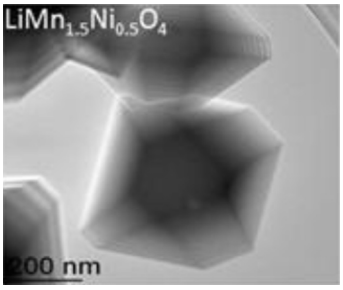

ARTICLE INFO

Article history:
Received 14 March 2014
Received in revised form
15 July 2014
Accepted 3 August 2014
Available online 11 August 2014

Keywords:
High voltage
Li-ion battery
Spinel cathode
Carbon coating

ABSTRACT

In this work, the high voltage $LiMn_{1.5}Ni_{0.5}O_4$ cathode material has been synthesized as octadecahedron crystals with a disordered spinel structure and has been coated with a carbon layer from two different precursors (sucrose and Xerogel carbon) to improve its performance in Li-ion batteries. The effect of carbon coating on the physical and electrochemical properties of the crystals has been evaluated using X-ray diffraction (XRD), Infrared (IR) and Raman spectroscopy, scanning electron microscopy (SEM), transmission electron microscopy (TEM), elemental and surface area (BET) analyses and battery cycling at different charge/discharge rates and temperatures. It was found that the amount of carbon, present as a thin layer (5–10 nm) and estimated at <1 w.t.%, causes an increase in electronic conductivity with no effect on crystal structure. Battery results of the cathode material in half cells show that carbon coating greatly improves the discharge capacity, rate capability at room temperature and 60 °C as well as cycling stability. Moreover, the material coated from Xerogel carbon shows the highest capacity at 10 C rate and 60 °C.

1. Introduction

There is a strong demand for safer, cheaper and more reliable Li-ion batteries with higher energy/power densities to power consumer electronic devices, power tools and electric vehicles. They are also needed to help stabilize and modernize the electrical grid and render it friendlier to the environment by integrating non-polluting energy sources such as wind and sun. One way to enhance energy density of a Li-ion battery is by increasing the voltage or/and capacity of the positive electrode, the cathode. The spinel $LiMn_{1.5}Ni_{0.5}O_4$, LMNO, cathode material has been identified as a promising candidate since the discovery that the substitution of the parent spinel $LiMn_2O_4$ with Ni for Mn cations shifts the potential of the redox reaction from 4.1 V vs. Li/Li^+ related to $Mn^{+3/+4}$ redox couple to 4.7 V vs. Li/Li^+ related to $Ni^{+2/}$

* Corresponding author.
E-mail addresses: Yaser.Abu-Lebdeh@nrc.gc.ca, yaser.abu-lebdeh@nrc-cnrc.gc.ca (Y. Abu-Lebdeh).

http://dx.doi.org/10.1016/j.jpowsour.2014.08.015
0378-7753/

$^{+4}$ couple where all the theoretical capacity (148 mAh g^{-1}) is delivered [1,2]. The material is also attractive because it has open 3D pathways that facilitate fast Li^+ ion diffusion and good rate capability. It also uses less toxic and cheaper metals than cobalt that is currently used in most electrodes in commercial batteries. However, it was realized that the battery performance of LMNO depends on many factors related to the material itself such as particle shape and size, crystalline structure (cation mixing and stoichiometry) and operating conditions such as electrolyte type, temperature and charge/discharge rates. Of particular concern is the poor battery performance at high rates and temperature, low discharge capacity and limited cycleability [3,4]. This is partly due to variations in electronic conductivity of different LMNO polymorphs and lithiated/delithiated phases and the high reactivity of the transition metal cations at the surface [5–7]. The latter leads to the formation of a thick, resistive passivation layer known as the cathode-electrolyte-interface, CEI, that can limit the electrochemical reaction (Li^+ ion intercalation and de-intercalation and associated charge transfer).

One popular approach to overcome the problem is to coat the material with either an inorganic compound such as an oxide, e.g. Bi_2O_3 [8], Al_2O_3 [9], TiO_2 [10], SiO_2 [11] or a phosphate, e.g. Li_3PO_4 [12], or their derivatives, e.g. BiOF [13] or LiPON [14]. This helps in protecting the electrolyte from the oxidative side reactions at high voltage but it does not directly improve the electronic conductivity. Coating with a thin layer of carbon is another method that has been successfully used for other cathode materials such as $LiFePO_4$, [15–17] $LiMn_{0.5}Ni_{0.5}O_2$ [18] and recently with LMNO [19]. This way the carbon coating tackles the two issues at once by protecting the electrolyte especially at high temperatures and most importantly enhancing the electronic conductivity. In this work, LiMNO was synthesized in an electrochemically favorable crystalline structure and shape and was coated with a carbon layer derived from Xerogel carbon along with sucrose for comparison. The results show that carbon coating especially from Xerogel carbon enhances the performance of LMNO as an electrode in half cells by increasing the rate capability and cycleability at room and high temperatures.

2. Experimental

2.1. $LiMn_{1.5}Ni_{0.5}O_4$ synthesis and carbon coating

The procedure used for the synthesis of LMNO was a slight variation of a sol–gel method described by Amine et al. [3], Wu & Kim [20], Zhong et al. [21] and our group [22,23]. In a typical synthesis, stoichiometric amounts of manganese acetate tetrahydrate (Aldrich), nickel nitrate hexahydrate (Aldrich) and lithium hydroxide monohydrate (Anachemia) were dissolved in distilled water. A small amount of carbon black was added as a stabilizing agent to the solution to prevent the formations of Mn_2O_3. The pH of solution was adjusted to pH 9–9.5 using ammonium hydroxide. The resulting mixture was stirred for 1 h at room temperature, before heating at 80 °C to form a viscous gel. This gel was then fired in air at 850 °C for 12 h and subsequently annealed at 600 °C for another 24 h and was let to cool at 5 °C min^{-1}.

For preparing carbon-coated LMNO from Xerogel carbon, the gel was first synthesized by reacting resorcinol (Aldrich) with formaldehyde (Aldrich) to give a dark-red gel as described by Cushing et al. [18]. LMNO powder was then combined with dried Xerogel Carbon in 80:20 weight ratio, ball-milled overnight and heated at 600 °C for 1 h in air. For carbon coating LMNO from sucrose, a predetermined amount of sucrose (1 w.t.%) was mixed with LMNO powder and the mixture was heated at 350 °C for 1 h in air as described by Yang et al. [19].

2.2. Physical characterization

X-ray powder diffraction patterns were obtained using a Bruker-AXS D8 diffractometer equipped with a CoKα ($\lambda = 1.79$ Å) radiation source and the angles were converted to the corresponding angles of CuKα ($\lambda = 1.54$ Å) using Bragg's law. The powders were scanned from 10° to 90° 2θ with a step size of 0.02° and step time of 1 s. The patterns were analyzed by the Rietveld refinement method using the software TOPAS v4.0 from Bruker AXS. The particle size and morphology of the powders were examined by SEM using a JEOL840A microscope operating at a voltage of 20 kV and a working distance of 15 mm. Chemical analyses was performed with a LEICO elemental analyzer to determine the amount of carbon. The specific surface area was estimated by nitrogen adsorption–desorption porosimetry at 77 K via the Brunauer–Emmet–Teller (BET) method using a Micromeritics ASAP2000 system. Prior to each measurement, the sample was evacuated overnight at 150 °C under a pressure of 10^{-6} torr. The transmission electron microscopy (TEM) analysis was performed on an FEI Titan-3 80–300 microscope equipped with a CEOS aberration corrector for the probe forming lens, as well as a monochromated field-emission gun. The images and the diffraction patterns were acquired on a CCD camera with a Gatan Imaging Filter (GIF 866). The diffraction patterns were acquired in energy-filtered mode to remove the contribution from inelastic scattering. The electronic conductivity of the powders was measured using an AC impedance spectroscopy technique. The powders were pressed into pellets at 3 metric tons with a diameter of 10 mm and then a conductive silver paint was spread on both sides of the pellets. The pellets were then sandwiched between two stainless steel electrodes in an in-house built conductivity cell. Raman spectra were obtained using a Renishaw inVia micro-Raman spectrometer equipped with a tunable laser with three different wavelengths: 514.5, 632.8, and 780 nm. The Attenuated Total Reflectance Infrared (ATR-IR) spectra were obtained using a Nicolet 6700 spectrometer from thermoscientific.

2.3. Electrochemical testing

Electrochemical evaluation was performed using 2325-type coin cells assembled in an argon filled glove box. The cathode film was prepared by mixing 76 w.t.% LMNO, 12 w.t.% Super S carbon (Timcal) and 12 w.t.% PVDF binder dissolved in N-methyl-pyrrolidone (NMP). The slurry was coated onto high purity aluminum foil and dried under vacuum at 110 °C overnight and individual 12.5 mm (0.50 inch) diameter electrode disks were punched out, and pressed. Lithium metal foils were used as a counter and reference electrode and 1 M $LiPF_6$ in ethylene carbonate: diethyl carbonate (EC:DEC, 3:7) was used as the electrolyte solution, together with microporous propylene separator (Celgard2500) for complete cell assembly. The cells were evaluated at room temperature and 60 °C in the voltage range 3.5–4.9 V. For the rate capability test, the cells were initially cycled at C/2 rate and then the rate increased gradually to 10 C. The capacities of the carbon-coated samples were not corrected to take into account the amount of carbon due to its low content that will have little effect on the capacity (<1 mAh g^{-1}).

3. Results and discussion

3.1. Materials synthesis and characterization

It was recently shown that LMNO with octahedron crystal morphology is kinetically more favorable for Li intercalation and de-intercalation and shows better rate capability in half cells [24]. Herein, LMNO was synthesized using a nitrate based sol–gel

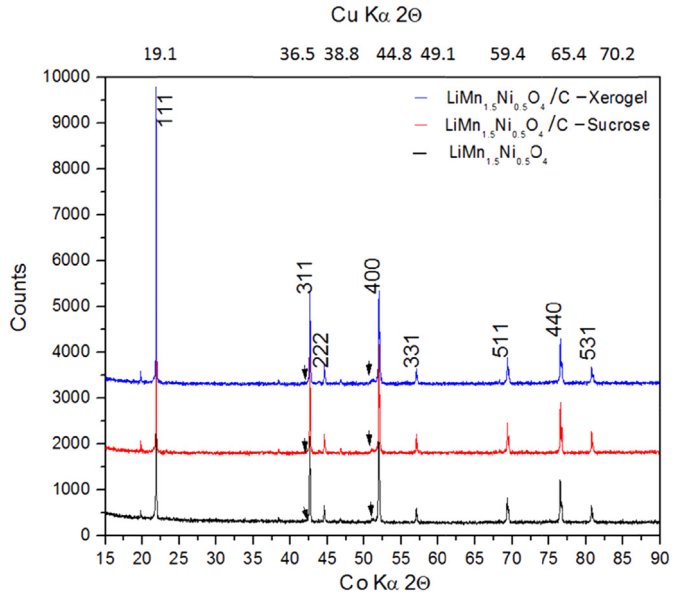

Fig. 1. SEM images, top, and high resolution TEM images, bottom, of $LiMn_{1.5}Ni_{0.5}O_4$ powders: bare (A), carbon-coated from sucrose (B) and carbon-coated from Xerogel Carbon (C).

method, denoted as bare from hereafter, and was coated from two different precursors. Fig. 1 shows the XRD patterns of the three LMNO powders. The main reflections in the three patterns can be indexed to cubic spinel structure with the disordered *Fd-3m* space group with the absence of reflections related to the $P4_332$ ordered space group which differ in the distribution of Ni and Mn cations within the octahedral sites. The disordered structure is believed to show better Li-ion diffusivity and electron transport than the ordered one resulting in improved battery performance [24]. The patterns show the presence of a minor impurity that can be assigned after close analysis to Ni_6MnO_8 rather than NiO [23] that is usually found in LMNO materials synthesized by the sol–gel method. The patterns show no evidence of diffraction peaks from carbon because it exists in a quantity below detection limits, as will be shown below, or it is amorphous. It also proves that heat treatment during carbon coating the powders did not result in any distortion to the crystal lattice. The lattice parameter was determined by a Rietveld refinement method and the values are shown in Table 1. They were consistent with reported values; 0.81721 nm, 0.81704 nm and 0.81701 nm for the bare LMNO, carbon-coated LMNO form Xerogel carbon and sucrose, respectively. The decrease in the lattice parameter for carbon-coated LMNO, although minute, can be attributed to the lower amount of Mn^{+3} (0.65 Å) in the structure which is larger than the Mn^{+4} (0.54 Å) as will be shown in the calculations from the 4.1 V plateau of the charge/discharge curves.

Fig. 2 shows the morphology of the three LMNO powders as observed by SEM. Image A of the bare LMNO shows that it is made of octahedron crystals of <111> facets with a large variation in size between 0.5 and 2 μm. However, on a closer look at the crystals using HR-TEM the image shows that the corners of the octahedron are not sharp but flattened giving rise to new facets that make the crystals octadecahedron in shape, Also, all the facets appear flat as judged by the thick fringes at the edges.

Coating the crystals with a carbon layer using sucrose or Xerogel carbon as a carbon source resulted in similar features to the bare LMNO as shown in images B and C of Fig. 2. However, the formation of agglomerates is pronounced and more significant in the case of LMNO coated from Xerogel carbon but in both cases no distinctive change in the microstructure of the LMNO crystals was observed. The HR-TEM images of the carbon-coated LMNO show the formation of a uniform, thin carbon layer at the surface of the crystal. The carbon layer is thinner in the case of LMNO coated from Xerogel carbon (~5 nm) than LMNO coated from sucrose (~10 nm). However, the bulk material showed also some carbon particles distributed among the crystals especially in the case of the LMNO coated from Xerogel carbon. This is consistent with what was observed by Cushing et al. [18] and Yang et al. [19] where adjacent thin, uniform carbon layers on layered or spinel LMNO derived from sucrose or Xerogel carbon can facilitate agglomeration of particles or crystals.

Fig. 3 shows the FT IR and Raman spectra of the bare and carbon-coated LMNO. The three samples show a similar IR pattern with the typical eight peaks in the range between 400 and 750 cm^{-1} characteristic of the disordered *Fd-3m* crystalline structure. This indicates that carbon coating did not affect cation ordering in the crystallographic structure of LMNO [10]. This was further corroborated by Raman spectra where the LMNO samples showed a similar pattern in the range between 100 and 700 cm^{-1} with the four broad peaks characteristic of the *Fd-3m* crystal structure of LMNO. Due to the small amount of carbon the Raman spectra in the range between 1300 and 1600 cm^{-1} showed very noisy and weak D and G bands that could not be used to evaluate the structure of the residual carbon, even when higher laser wavelengths (632.8 and 780 nm) were tried.

The amount of carbon left at the surface of carbon-coated LMNO after heating at 350 °C and 600 °C were calculated as described by Cushing et al. [18] and the results are summarized in Table 1. The bare LMNO has no residual carbon but as the manganese precursor is the organic anion acetate there might be some carbon traces that are below the detection limit of the instrument. The amount of carbon in the LMNO coated from sucrose was 0.68 w.t.% that is slightly lower than the 0.73 w.t.% found in the LMNO coated from Xerogel carbon despite the much higher amount of carbon precursor (20% vs. 1%). This is slightly lower than what was reported for the layered oxide $LiMn_{0.5}Ni_{0.5}O_2$ using the same amount of Xerogel carbon [18]. These low amounts of carbon are sufficient to show a positive effect on the battery performance of LMNO and no further optimization was attempted to increase them. In general, the amount and type of carbon in a cathode should be balanced so it does not hinder Li-ion transport or be involved in side reactions with the electrolyte especially at such high voltages or act as a reducing agent for metal cations at the surface. It is widely accepted from studies on other cathode materials that, with the right particle size, only small amounts (<5 w.t.%) of highly conductive, porous

Table 1
Summary of the physical properties of bare and carbon-coated $LiMn_{1.5}Ni_{0.5}O_4$ powders.

Carbon precursor	Amount of precursor (%)	Amount of carbon (%)	BET surface area ($m^2\ g^{-1}$)	Lattice parameter (nm)	Electronic conductivity ($S\ cm^{-1}$)
Bare LMNO	none	none	1.3	0.81721	5.2×10^{-7}
LMNO coated from sucrose	1	0.68	0.9	0.81701	4.1×10^{-6}
LMNO coated from Xerogel carbon	20	0.73	1.1	0.81704	9.5×10^{-6}

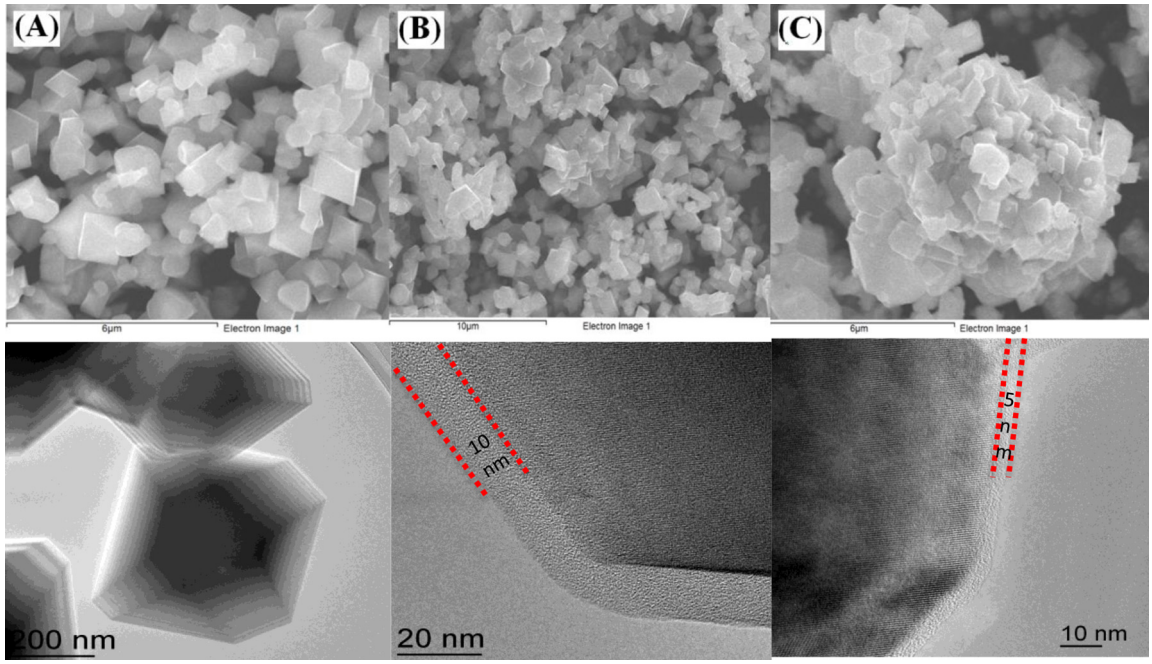

Fig. 2. XRD patterns of bare and carbon-coated $LiMn_{1.5}Ni_{0.5}O_4$ powders.

carbon are needed to have a positive effect on the battery performance specially at high cycling rates [19]. Carbon enhances the electronic conductivity of electrode materials by providing conductive paths for the electrons and, in a different mechanism, it could reduce Mn^{+4} surface species to Mn^{+3} leading to $Mn^{+3/+4}$ conductive pathways. Yang et al. [19] showed by XPS measurements that the latter is not the case in LMNO coated from sucrose, possibly due to the low content of carbon which could also apply to the LMNO coated from Xerogel carbon synthesized in this work [19]. There is also the possibility that the porous structure of carbon layer could act as a reservoir for the electrolyte. This keeps excess electrolyte close to the surface resulting in faster electrochemical reactions and improved battery performance.

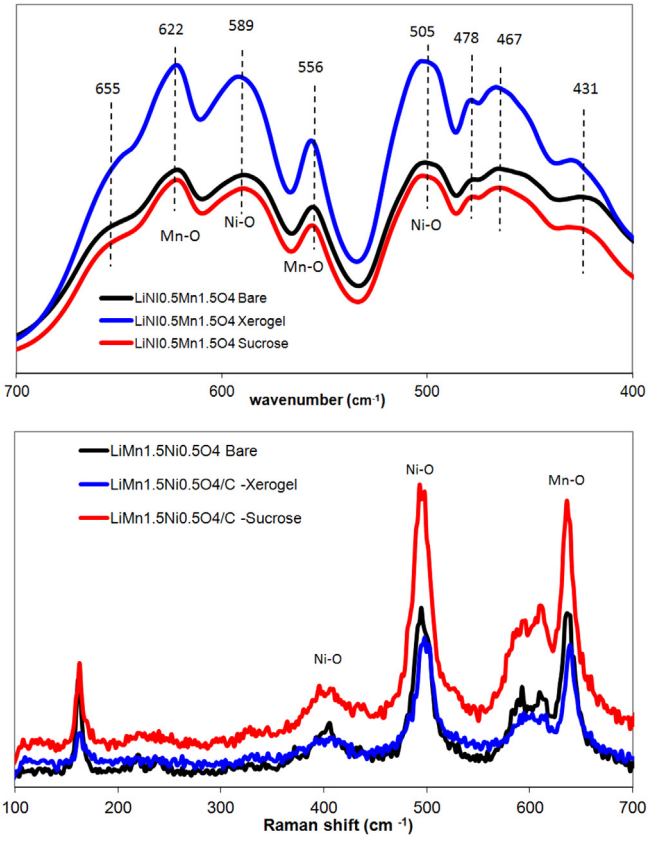

Fig. 3. IR (top) and Raman (bottom) spectra of the bare and carbon-coated $LiMn_{1.5}Ni_{0.5}O_4$ powders.

The electronic conductivity was measured for the three LMNO powders, made into pellets, and the results are also shown in Table 1. The conductivity increased slightly from 5.2×10^{-7} S cm^{-1} for the bare LMNO to 4.1×10^{-6} S cm^{-1} for LMNO coated from sucrose, similar to what was observed by Yang et al. [19], and significantly to 9.5×10^{-6} S cm^{-1} for the LMNO coated from Xerogel carbon. The higher conductivity of the LMNO samples coated from Xerogel carbon can be explained not only by the slightly higher amount of carbon, that could be of a more conductive nature, but also by the presence of carbon agglomerates, as evidenced by SEM and TEM, that could form percolation pathways for electrons. The importance of carbon coating LMNO is to keep a high electronic conductivity during the delithiation process. It was shown recently that significant drop in electronic conductivity of disordered LMNO polymorph by more than two orders of magnitude takes place during the first stage of de-lithiation at 4.1 V due to Mn^{+4} to Mn^{+3} conversion [7]. It is worth mentioning that due to variation in the morphology of the three samples and the complexity of impedance measurements, the conductivity values should be treated with caution and are shown here to emphasize a trend.

The surface area of the bare and coated LMNO was calculated using BET analysis and the values are also shown in Table 1. The Surface area of the bare LMNO was 1.3 m^2 g^{-1} decreasing to 1.1 m^2 g^{-1} for the LMNO coated from Xerogel carbon and to 0.9 m^2 g^{-1} for LMNO coated from sucrose. The value for the bare LMNO is consistent with what is reported for similar LMNO crystals prepared by Hai et al. (1 m^2 g^{-1} for octahedron crystals with 2 μm average size) [24], but slightly higher due to the higher number of facets in the octadecahedron than the octahedron crystals. The

decrease in surface area of carbon-coated LMNO is a result of agglomeration of crystals into larger aggregates with irregular shapes facilitated by the surface carbon layer, as seen in some carbon-coated cathode materials [19].

3.2. Electrochemical and battery performance

The electrochemical performance of bare and coated LMNO was evaluated in Li/LMNO half cells using 1 M $LiPF_6$ in EC:DEC (3:7) electrolyte solution. Fig. 4 compares charge–discharge curves of the three LMNO materials at a cycling rate of C/2 for the first cycle. As can be seen, all profiles exhibited distinctive, flat charge and discharge plateaus at 4.7 V region related to the reversible electrochemical reaction of $Ni^{+2/+4}$ redox couple. Another very short plateau at 4.1 V vs. Li/Li^+ related to $Mn^{+3/+4}$ redox couple was also observed. The shapes of the charge/discharge curves are not conclusive but they seem to support a solid-solution rather than a two-phase lithiation/de-lithiation mechanism, characteristic of the disordered polymorph [25]. The carbon-coated LMNO showed higher discharge capacities reaching 140 mAh g^{-1} than bare LMNO with 110 mAh g^{-1}. The coated LMNO showed slightly lower voltage difference between charge and discharge due to the lower surface area and polarization. The capacities obtained at the short plateau at 4.1 V vs. Li/Li^+ were used to calculate the amount of Mn^{+3} present in LMNO and the ratio was estimated to be 3.6% for the bare LMNO and 2.7% for the coated LMNO. This is consistent with what was observed by Hai et al. who reported the presence of only 1.5% of Mn^{+3} (calculated at C/22) in octahedron crystals that showed a slightly higher capacity of ~130 mAh g^{-1}at C/2 than the bare LMNO crystals reported in this work [24]. The two carbon-coated LMNO samples showed a similar irreversible capacity of 13 mAh g^{-1} lower than the bare LMNO at 20 mAh g^{-1} and higher discharge capacity at 125 mAh g^{-1} than the bare LMNO at 115 mAh g^{-1}. The effect of Mn^{+3} on the battery performance is therefore still not clear due to the difficulty in comparing the performance of LMNO materials prepared by different synthetic procedures which results in different types and amounts of impurities and surface composition. The capacity of the bare LMNO is lower by approximately 20 mAh g^{-1} than some reported values which is expected due to the use of lower amount of carbon additive 12 w.t.% and conventional binder in this work compared to double the amount of carbon additive used by Liu et al. [10] or the use of conductive binder by Kim et al. [26]. It is important in this work to keep the carbon additive amount low in order to easily emphasize the effects of carbon coating on the battery performance of LMNO.

To examine the effect of carbon coating on the rate capability of LMNO, the half cells were charged from C/2 to 10 C rate then back to C/2 and discharged at identical rates and the results are shown in Fig. 5. It can be seen that at all rates the discharge capacities were higher for the carbon-coated LMNO than the bare one. In the region between C/2 to 5 C rate an increase of 20–30% in capacity was observed while at 10 C the effect is more prominent as the bare LMNO showed almost no capacity (5 mAh g^{-1}) while the carbon-coated ones still show half the capacity at C/2 (60–70 mAh g^{-1}). Moreover, at lower C-rate LMNO coated from sucrose gave higher capacities than LMNO coated from Xerogel carbon while the latter gave higher capacities at higher C-rate (10 C) and the two recovered at C/2 with 98% capacity retention after 100 cycles. Yang et al. showed a similar increase in discharge capacity of the bare LMNO upon coating with carbon from sucrose using a similar LMNO:sucrose ratio, showing double the capacity retention at 5 C (114 mAh g^{-1}) compared to the bare electrode [19]. Also, the figure shows that cycleability was enhanced as after 100 cycles more than 92% of capacity was retained in the carbon-coated LMNO compared to the bare LMNO with only 62%. Ma et al. [27] showed that large crystal/particles (>1 μm), similar to the ones reported in this work, do not limit rate capability indicating fast electron and Li-ion diffusivity within the crystal while Ariyoshi et al. [28] showed that larger particles made by increasing calcination temperature show in general lower polarization. Liu et al. [10] showed that other processes such as phase transformation ($LiMn_{1.5}Ni_{0.5}O_4/Li_{0.5}Mn_{1.5}Ni_{0.5}O_4/Mn_{1.5}Ni_{0.5}O_4$) and charge/discharge transfer could play a role. This demonstrates that the observed enhancement in LMNO performance at high cycling rates due to carbon coating could be attributed to improvements in bulk and interfacial (current collector/electrode/electrolyte) properties of the electrodes rather than changes within the crystal/particle. Fig. 5 also shows that LMNO coated from Xerogel gives better performance and able to extend the rate capability to higher C-rate (10 C) than the bare or LMNO coated from sucrose, possibly due to the much higher electronic conductivity and the thinner carbon layer that allow for faster electrochemical reactions and less electrolyte decomposition. The coulombic efficiency of the three electrodes are also shown in Fig. 5 and they all show efficiencies close to 98%. The bare LMNO showed a large drop in efficiency that fluctuated on cycling at 10 C that could not be seen in the coated samples. This emphasizes the

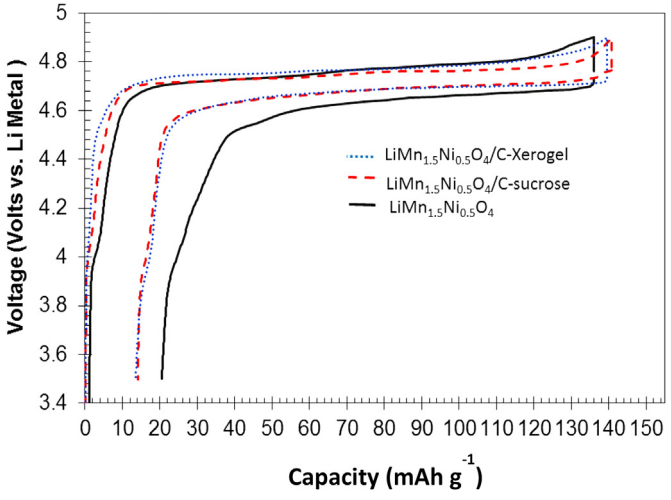

Fig. 4. Voltage–capacity curves at room temperature and C/2 rate of the first cycle for the bare and carbon-coated $LiMn_{1.5}Ni_{0.5}O_4$ using 1 M $LiPF_6$ in EC:DEC 3:7 as electrolyte and lithium foil as counter and reference electrode.

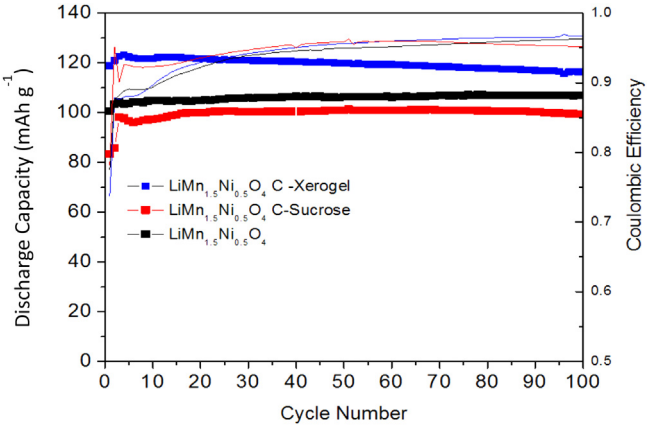

Fig. 5. Discharge capacities and Coulombic efficiencies at room temperature and different rates for the bare and carbon-coated $LiMn_{1.5}Ni_{0.5}O_4$ using 1 M $LiPF_6$ in EC:DEC 3:7 as electrolyte and lithium foil as counter electrode.

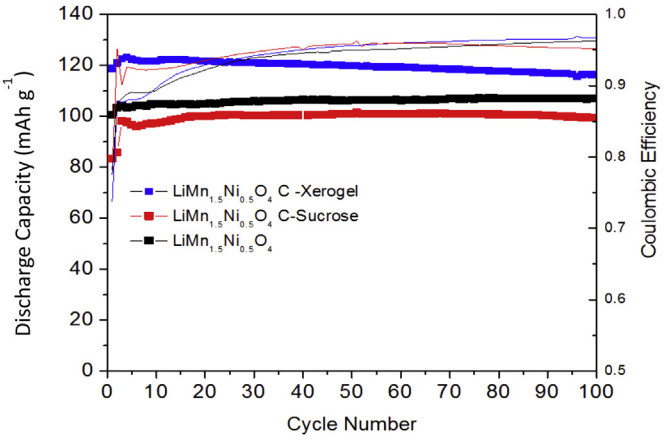

Fig. 6. Discharge capacities and Coulombic efficiencies at 60 °C and C/2 rate for the bare and carbon-coated $LiMn_{1.5}Ni_{0.5}O_4$ using 1 M $LiPF_6$ in EC:DEC 3:7 as electrolyte and lithium foil as counter and reference electrode.

importance of thin carbon coating for this type of material at higher C-rates and its role in mitigating the effect of polarization and side reactions.

To investigate the effect of temperature on the battery performance of LMNO, the half cells were tested at 60 °C and the results are shown in Fig. 6. Again, LMNO coated from Xerogel carbon showed the best performance by giving the highest capacities at C/2 over 100 cycles. It showed a discharge capacity of 125 mAh g^{-1} and 95% capacity retention after 100 cycles compared to 110 mAh g^{-1} for the bare LMNO and 100 mAh g^{-1} for LMNO coated from sucrose with 97%–98% capacity retention, respectively. This shows that LMNO coated from Xerogel carbon works better than LMNO coated from sucrose at high temperature. This is probably due to the formation of a more robust, passivating CEI film that prevents side reactions with the electrolyte that can be triggered by the high temperature [29,30]. The Coulombic efficiency is also presented in Fig. 6 and shows that the efficiencies were slightly lower than those at room temperature. It shows also that they were low at the first cycles but increased gradually, with LMNO coated from sucrose giving the lowest values after 100 cycles reaching 95%. This partly explains the drop in capacity of LMNO coated from sucrose at high temperature to values lower even than those of the bare. It suggests a decomposition of the carbon coating and onset of side reactions with the catalytic metal cations at the surface of LMNO. This could be related to the thickness of the carbon layer, being thinner in the case of the LMNO coated from Xerogel.

Finally, the process for carbon coating LMNO in this work involves ball-milling of bare LMNO with carbon, and heating at 600 °C for 1 h. That might pulverize and homogenize the final LMNO materials, which could lead to improvement in electrochemical performances even without the carbon coating. In order to decouple the effect of the processing conditions from the effect of carbon coating on the performance of the bare LMNO, a comparison was made by firstly ball-milling a bare LMNO and secondly ball-milling and heating a bare LMNO at 600 °C for 1 h without carbon precursors. The XRD, IR and Raman spectra looked exactly similar to the bare LMNO indicating no effect on the crystal structure, cation ordering, of the spinel LMNO. Batteries were also assembled and tested at similar rates to the bare and carbon-coated LMNO. They showed capacities slightly higher than the bare LMNO at initial cycling but drop to values similar to bare LMNO, overall much lower than the values for the carbon-coated LMNO.

4. Conclusions

It was demonstrated in this work that carbon coating of the high voltage $LiMn_{1.5}Ni_{0.5}O_4$ cathode material can successfully enhance its battery performance. It was successfully synthesized as octadecahedron crystals with disordered spinel structure by a sol–gel method and carbon-coated from Xerogel carbon or sucrose as precursor resulting in thin coatings (5–10 nm) that increased its electronic conductivity. Battery testing showed that the carbon-coated materials gave higher capacities at room temperature than the bare material. Also, the material coated from Xerogel carbon gave higher capacity at high C-rate (10 C) indicating higher electronic conductivity and thinner coating, and at 60 °C indicating the formation of a protective passivation layer.

Acknowledgment

The authors would like to thank Amy Hrdina, Steve Argue, David Kingston and Floyd Toll for their technical assistance. The authors acknowledge Natural Resources Canada for partial funding through the Office of Energy Research and Development.

References

[1] Q. Zhong, A. Bonakdarpour, M. Zhang, Y. Gao, J.R. Dahn, J. Electrochem. Soc. 144 (1997) 205.
[2] K. Amine, H. Tukamoto, H. Yasuda, Y. Fujita, J. Power Sources 68 (1997) 604.
[3] K. Amine, H. Tukamoto, H. Yasuda, Y. Fujita, J. Electrochem. Soc. 143 (1996) 1607.
[4] S. Patoux, L. Daniel, C. Bourbon, H. Lignier, C. Pagano, F. Le Cras, S. Jouanneau, S. Martinet, J. Power Sources 189 (2009) 344.
[5] J.C. Arrebola, A. Caballero, L. Hernan, J. Morales, J. Power Sources 195 (2010) 4278.
[6] T. Noguchi, I. Yamazaki, T. Numatta, M. Shirakata, J. Power Sources 174 (2007) 359.
[7] R. Amin, A. Rasil, D. Ravnsbaek, Y.-M. Chiang, 223rd ECS Meeting, 2013. Abstract number 153.
[8] J. Liu, A. Manthiram, Chem. Mater. 21 (2009) 1695.
[9] R. Alcantara, M. Jaraba, P. Lavela, J. Tirado, J. Electroanal. Chem. 566 (2004) 187.
[10] J. Liu, A. Manthiram, J. Electrochem. Soc. 156 (2009) A833.
[11] J. Liu, A. Manthiram, J. Electrochem. Soc. 156 (2009) A66.
[12] Y. Kim, N.J. Dudney, M. Chi, S.K. Martha, J. Nanda, G.M. Veith, C. Liang, J. Electrochem. Soc. 160 (2013) A3113.
[13] H.-B. Kang, S.-T. Myung, K. Amine, S.-M. Lee, Y.-K. Sun, J. Power Sources 195 (2010) 2023.
[14] S. Seki, Y. Kobayashi, H. Miyashiro, Y. Mita, T. Iwahori, Chem. Mater. 17 (8) (2005) 2041.
[15] Z. Chen, J.R. Dahn, J. Electrochem. Soc. 149 (9) (2002) A1184.
[16] K. Wang, R. Cai, T. Yuan, X. Yu, R. Ran, Z. Shao, Electrochim. Acta 54 (2009) 2861.
[17] D.D. MacNeil, L. Devigne, C. Michof, I. Rodrigez, G. Liang, M. Gauthier, J. Electrochem. Soc. 157 (4) (2010) A463.
[18] B.L. Cushing, J.B. Goodenough, Solid State Sci. 4 (2002) 1487.
[19] T. Yang, N. Zhang, Y. Lang, K. Sun, Electrochim. Acta 56 (2011) 4058.
[20] X. Wu, S.B. Kim, J. Power Sources 109 (2002) 53.
[21] Q. Zhong, A. Bonakardarpour, M. Zhang, Y. Gao, J. Dahn, J. Electrochem. Soc. 144 (1997) 205–213.
[22] S. Niketic, P.S. Whitfield, I.J. Davidson, Yaser Abu-Lebdeh, in preparation.
[23] B. Hai, A.K. Shukla, H. Duncan, G. Chen, J. Mater. Chem. A 1 (2013) 759.
[24] H. Duncan, Y. Abu-Lebdeh, I.J. Davidson, J. Electrochem. Soc. 157 (2010) A528.
[25] A. Manthiram, K. Chemelewski, E.-S. Lee, Energy Environ. Sci. 7 (2014) 1339.
[26] J.-H. Kim, S.-T. Myung, C.S. Yoon, S.G. Kang, Y.-K. Sun, Chem. Mater. 16 (5) (2004) 906.
[27] X. Ma, B. Kang, G. Ceder, J. Electrochem. Soc. 157 (2010) A925.
[28] K. Ariyoshi, Y. Maeda, T. Kawai, T. Ohzuku, J. Electrochem. Soc. 158 (2011) A281.
[29] H. Duncan, D. Duguay, Y. Abu-Lebdeh, I.J. Davidson, J. Electrochem. Soc. 158 (2011) A537.
[30] H. Duncan, N. Salem, Y. Abu-Lebdeh, J. Electrochem. Soc. 160 (2013) A838.